Supporting Information

Fluorinated polymer zwitterions on gold nanoparticles: patterned catalyst surfaces guide interfacial transport and electrochemical CO_2 reduction

Qiang Luo,[1] Joseph Tapia,[5] Le Zhou,[4] Chung-Hao Liu,[2,6] Maham Liaqat,[1] Hanyi Duan,[2] Zhefei Yang,[4] Mu-Ping Nieh,[2,3] Todd Emrick*,[4] Peng Bai,*,[5] and Jie He*,[1,2]

[1]Department of Chemistry, [2]Polymer Program, Institute of Materials Science, and [3]Department of Chemical and Biomolecular Engineering, University of Connecticut, Storrs, CT 06269, United States.
[4]Polymer Science and Engineering Department, Conte Center for Polymer Research and [5]Department of Chemical Engineering, University of Massachusetts, Amherst, Massachusetts 01003, United States.
[6]Neutron Scattering Division, Oak Ridge National Laboratory, Oak Ridge, Tennessee 37831, United States.
Emails: tsemrick@mail.pse.umass.edu (TE), pengbai@umass.edu (PB) and jie.he@uconn.edu (JH)

Contents

1. Chemicals and materials.
2. Synthesis of polymer zwitterions.
3. Synthesis of citrate capped AuNPs and Au/C.
4. Surface ligands modifications of AuNPs with various polymers.
5. *In-situ* ATR-SEIRAS measurements.
6. Electrochemical measurements.
7. Determination of grafting density.
8. Determination of diffusion coefficients using molecular probes.
9. Other characterizations.
10. Molecular dynamics (MD) simulations.

Figure Contents

Supporting Figure S1. Summary of polyzwitterions.

Supporting Figure S2. FT-IR spectra of ligands P1, P2, P3 and Au NPs modified with P1, P2, P3.

Supporting Figure S3. TGA thermograms of ligands including P1, P2, P3, Au nanocatalyst and functionalized Au NPs with ligands including P1, P2 and P3.

Supporting Figure S4. Electronic microscopy characterization of Au/C.

Supporting Figure S5. Electrocatalysis results of Au/C modified with various ligands.

Supporting Figure S6. LSV curves of unmodified Pd/C and one modified with P3.

Supporting Figure S7. SEIRAS spectra of Au modified with P1 and P2.

Supporting Figure S8. .SAXS patterns of various polymer zwitterions modified Au film substrate.

Supporting Figure S9. MD simulations of the ligands on the local solvated CO_2 around work electrode.

Supporting Figure S10. MD simulations of the ligands on the local solvation environment to work electrode.

Supporting Figure S11. Comparison of localized water structures modified with various ligands.

Supporting Figure S12. CV curves of Au NPs and ligands modified Au NPs in the presence of $K_3Fe(CN)_6$.

Supporting Figure S13. CV curves of Au NPs and ligands modified Au NPs in the presence of $Ru(NH_3)_6Cl_3$.

Supporting Figure S14. CV curves of Au NPs and ligands modified Au NPs in the presence of Fc-COOH.

Supporting Figure S15. EIS measurements of Au NPs and one modified with ligands including P1, P2 and P3.

Supporting Figure S16. MD simulations of CO_2 motion.

Supporting Table S1. ECSA results summary of Au/C without polymer modification.

Supporting Table S2. ECSA results summary of P1-Au/C.

Supporting Table S3. ECSA results summary of P2-Au/C.

Supporting Table S4. ECSA results summary of P3-Au/C.

Supporting Table S5. FE of Au NPs modified with polymer zwitterions and other Au catalysts.

Supporting Table S6. FE results summary of Pd/C and P3-Pd/C.

1. Chemicals

Gold(III) chloride trihydrate ($HAuCl_4 \cdot 3H_2O$), potassium bicarbonate ($KHCO_3$), ethanol (anhydrous, ≥99.5%), 2,2,2-trifluoroethanol, sodium citrate tribasic dihydrate (≥99.0%), sodium hydroxide (NaOH, ≥99.0%), potassium bicarbonate ($KHCO_3$, ≥99.5%), was purchased from Sigma Aldrich. Printex U activated carbon was kindly gifted from Orion. Deionized water (High-Q, Inc. 103S Stills) with a resistivity of >10.0 MΩ was used in all experiments. Commercially available Pd/C (Pd loading: 5 wt%) were obtained from Alfa-Aesar. 2-Methacryloyloxyethyl phosphorylcholine (MPC), 4,4'-azobis(4-cyanovaleric acid) (98%, ACVA) and 4-cyano-4-(phenylcarbonothioylthio)pentanoic acid (CPPA) (>97%) were purchased from Sigma Aldrich. 2,2,2-Trifluoroethanol (TFE) was purchased from Oakwood Chemical. The fluorinated choline phosphate (FCP) monomers were prepared as previously reported.[1-2]

2. Synthesis of polymer zwitterions

Homopolymers P1-P3 were prepared by reversible addition−fragmentation chain-transfer polymerization.[1] The chain transfer agent 4-CPPA, ACVA ([CPPA]:[ACVA] = 1:0.2), FCP or MPC monomer (50 equiv) and TFE were added to a 20 mL glass vial sealed with a rubber septum. The reaction mixture was purged with N_2(g) for 25 min and then stirred at 70 ^oC for 13 h, after which the vial was submerged into N_2(l) to quench the polymerization. Monomer conversion was determined from ^1H NMR of aliquots taken from the polymerization crude, by integrating alkene signals of residual monomer against peaks arising from polymer backbone or sidechain. Typical monomer conversion for the homopolymerizations was 80-95%. The polymerization crude was diluted with TFE prior to precipitation. PMPC and poly (HFIP-MCP) were obtained by precipitation in diethyl ether, dialysis against deionized water, and lyophilization. Poly (PFO-MCP) was purified by precipitation into a mixture of acetone and diethyl ether(once), acetone (once) and diethyl ether (once) and drying in vacuo. The polymers were isolated as pink solid in ~80% yield.

3. Synthesis of citrate capped AuNPs and Au/C

3.1 AuNPs

Citrate-capping Au NPs (diameter 3.2±0.6 nm) were synthesized using a method reported previously.[3] Briefly, a 100 mL of aqueous solution containing 10 mg of $HAuCl_4$ and 9 mg of trisodium citrate was prepared in a flask. Then, 1.5 mL of ice-cold, freshly prepared 0.2 M $NaBH_4$ solution was added to the

solution while stirring (900 rpm). Consequently, the solution turned to pinkish color immediately after injection of $NaBH_4$ solution. This indicated the formation of Au nanoparticles growth in the flask. After stirring for 2 hours, the synthesized Au NPs was ready for further use without purification.

3.2 Au/C

For the catalyst Au/C synthesis, AuNPs were loaded onto activated carbon (Printex U, 50 nm). Initially, activated carbon (30 mg) was dispersed in 10 mL of ethanol through 45 minutes of sonication process. Subsequently, the above mixture was then combined with 30 mL of the synthesized Au stock solution (0.1 mg mL^{-1}) and following another sonication for 30 minutes. After stirring overnight and following centrifugation process, the Au/C catalyst with a loading amount of 2.5 wt% AuNPs was obtained. Finally, the Au/C catalysts were collected after dried under vacuum overnight.

4. Surface ligands modifications of AuNPs with various polymers

Generally, a 5 mL solution containing Au/C (with a 2.5 wt% gold loading) in methanol (1 mg mL^{-1}) was first introduced into another 2 mL of aqueous solution containing polymer (P1) (1 mg mL^{-1}) while stirring and reacting overnight for overnight. Consequently, the Au/C catalysts after modification were purified using methanol three times to remove free polymers and collected after drying under vacuum. Similarly, the surface modification of P2 and P3 was carried out with the same method except using trifluoroethanol as a solvent.

5. *In-situ* SEIRAS measurement

A 60° Si ATR crystal with a gold film was used as the working electrode for all measurements in 0.1M $KHCO_3$ electrolyte. The Si ATR crystal was polished using various alumina suspensions (1.0, 0.3, and 0.05 μm from Buehler) and then sonicated in water and acetone three times to remove any silica residuals. The Si ATR crystal was polished using various alumina suspensions (1.0, 0.3, and 0.05 μm from Buehler) and then sonicated in water and acetone three times to remove any silica residuals. Afterward, it dried under N_2 flow before using for the next step with film deposition.

Then, the Si crystal was immersed in piranha solution (3:1 volume ratio of H_2SO_4 (95–98 wt.%) and H_2O_2 (30 wt.%)) for 25 minutes to remove organic contaminants from the surface. To improve adhesion properties before Au film growth, the Si prism was immersed in a 40 wt.% NH_4F solution for 2 minutes,

followed by rinsing with DI water. The process for preparing the Au film was adapted from previous literature with modifications.[4-5] Briefly, 50 mL of Au plating solution was prepared by mixing two solutions under sonication: 1) 0.3 M Na_2SO_3 + 0.1 M $Na_2S_2O_3$ + 0.1 M NH_4Cl (45mL)and 2) 0.03 M $HAuCl_4 \cdot 3H_2O$, 0.026 M NaOH (5mL). Then, the Si prism was partially soaked into the plating solution, composed of HF (2 wt.%) and Au plating solution with volume ratio of 1:4.4 at around 55 °C for 3 min. Notably, the growth period of the Au film is highly dependent on the temperature of the water bath. Therefore, maintaining a stable temperature is critical for obtaining a high-quality film to be used as a working electrode later. Subsequently, a bright gold-colored surface on a Si prism was obtained. Finally, the Au film working electrode was rinsed three times with DI water to eliminate any residual Au plating solution. The working electrode was then dried under N_2 before measurement.

In this project, the ATR-SEIRAS experiments were carried out by employing a Nicolet iS50 Fourier transform infrared (FTIR) spectrometer attached with an ATR accessory VeeMAX III from Pike Technologies combined with a liquid nitrogen-cooled mercury cadmium telluride (MCT) detector. Before taking measurements, N_2 was saturated into all the accessory chambers for 3 h to establish a stable background and prevent moisture from the surroundings. Similarly, the Au film working electrode was electrochemically activated through cyclic voltammetry (CV) scans at ambient conditions ranging from -0.3 to 0.65 V in 0.1M $KHCO_3$ at 50 mV s^{-1} until it reached stability. The single-beam spectrum before electrocatalysis was used as a background in absorbance units (a.u.) to represent an increase in interfacial species and ligands, while negative values indicate a decrease. The 16-scans with a resolution of 4 cm^{-1} were used for spectrum collection. All potentials used here were reported in the reversible hydrogen electrode (RHE) scale.

6. Electrochemical measurements

This study employed a pyrolytic graphite (PG) electrode to load the catalyst ink as the working electrode, a saturated calomel electrode (SCE) as the reference electrode, and a carbon rod as the counter electrode. Electrochemical studies were conducted using a CH Instrument 627E potentiostat throughout all experiments. A catalyst was prepared by sonicated a mixture ink compose of 5 mg of the catalyst, 200 µL of isopropanol and 1000 µL of H_2O continuously for 30 min prior for utilizing as a catalyst ink. Then, a volume of 10 µL ink was deposited onto the PG electrode following with through drying under a nitrogen atmosphere over 45 min. Electrochemical CO_2 reduction studies were performed on several

Au/C catalysts using a customized H-cell setup. The reaction cell was divided into cathode and anode compartments using a Nafion membrane. Both sides of the H-cell were filled with 27 mL of $KHCO_3$ (0.1 M) electrolyte, leaving 11 mL of headspace for electrocatalysis. Prior to electrocatalysis, CO_2 was continuously purged for 30 min to saturate the solution and remove any other gaseous species. Linear sweep voltammetry (LSV) scans were conducted over a potential range of -0.2 to -1.2 V, with a scan rate of 10 mV s^{-1}. All potentials here were described in reversible hydrogen electrode (RHE) values using the equation, $E_{RHE} = E_{SCE} + 0.244\ V + 0.0591 \times pH$.

To evaluate efficiency and durability of an electrocatalyst, chronoamperometry technique, also known as current-time (i-t) analysis, was employed under different potentials. Gas chromatography (GC) was employed to evaluate the reduction products.

For the characterization of electrochemical active surface area (ECSA) for nanocatalysts, we measured the CVs of catalysts in a N_2-saturated H_2SO_4 (0.5 M) solution with a scan rate of 100 mV s^{-1}. The ECSAs of all Au catalysts could be obtained through the reduction peak of the surface generated oxide layers at -1.15 V with 390 μC·cm^{-2} as a reference charge value for Au. The following equation could be used to calculate the ECSAs.[6]

$$\text{Charge} = \frac{Area\ of\ Au\ reduction\ peak}{Scan\ rate}$$

$$\text{ECSA} = \frac{Charge}{390\ \mu C \cdot cm^{-2}}$$

7. Determination of polymer grafting density

For the grafting density of polymer zwitterion upon AuNPs, thermogravimetric analysis (TGA) analysis was examined carefully for all polymer-modified Au/C nanocatalysts under N_2 atmosphere based on the equation shown below. [7]

$$\text{polymer chains / NPs} = \frac{the\ total\ number\ of\ polymer\ chains}{the\ total\ surface\ area\ of\ Au\ NPs}$$

where the total number of polymer chains was calculated using $\frac{m_{polymer} \times N_A}{M_{polymer}}$, while the total surface area could be figured out from $S_{NP} \times \frac{\frac{m_{Au}}{M_{Au}}}{\rho_{Au} \times \frac{V_{NP}}{M_{Au}}}$. Specifically, N_A is the Avogadro constant. ρ_{Au} is the density of

bulk Au materials. S_{NP} and V_{NP} refer to the surface area and volume of an individual Au NP. $m_{polymer}$ and m_{Au} refers to the mass of polymer zwitterions and AuNPs, respectively while $M_{polymer}$ and M_{Au} are molecular weight of polymer zwitterions and Au atoms, respectively.

Using Au-P1/C catalysts as an example for the grafting density estimation. From TGA decomposition curves, a weight loss of 74.5 wt% was obtained compared to initial mass of polymer over 700 °C. Then, an Au/C nanocatalyst without polymer zwitterions was characterized to deduce the background with a weight loss of 11.9 wt% under identical examination condition. Consequently, the mass loss could be calculated out, (15.7wt%-11.9wt%)/74.5wt% =5.1wt%. Afterwards, the grafting mass of P1 was obtained through 1.69 mg×5.1 %= 0.086 mg. Then, the grafting density of P1 could be obtained shown as follow:

Total # of Au NPs = $\frac{\frac{mAu}{M\,Au}}{\rho Au \times \frac{VNP}{MAu}} = \frac{\frac{0.04\ mg}{196\ g\ mol^{-1}}}{19.3\ g\ cm^{-3} \times \frac{1.4\times10^{-26} m^3}{196\ g\ mol^{-1}}} = 1.48 \times 10^{14}$

Surface area of Au NPs = $4\pi r_{Au^2} = 4\times3.14\times (1.5 \times 10^{-9}\ m)^2 = 28.3\ nm^2$

Total # of polymer chains = $\frac{m_p}{Mp} \times \text{NA} = \frac{0.086\ mg}{16300\ g\ mol^{-1}} \times 6.022 \times 10^{23} = 3.19 \times 10^{15}$

Finally, the grafting density of P1 = $\frac{3.19\times10^{15}}{28.3\ nm^2\times1.48\times10^{14}} = 7.6 \times 10^{-1}\ chains/nm^2$

Likewise, the grafting density of P2 on Au/C could be obtained through two TGA curves including P2-Au/C and unmodified Au/C as blank background (Figure S3). Specifically, the weight loss of P2 is 14 wt% at 700 °C. Then, the mass loss could be calculated as (14 wt%-11.9 wt%)/76.5 wt% =2.7 wt%. With the initial loading amount of P2-Au/C nanocatalyst, the grafting mass of P2 was 0.035 mg. Following the same method, the total number of polymer chain and Au NPs could be calculated out with 9.79×10^{14} and 1.15×10^{14}. respectively. Finally, the grafting density of P2 could be calculated with 0.30 chains/nm^2. Similarly, for grafting density of P3, the weight loss of P3 is 84.8 wt% over 700 °C with mass loss of (16.4 wt%-11.9 wt%)/84.8 wt% =5.3 wt%. Based on the initial loading amount of nanocatalyst for TGA examination (Figure S3), the grafting mass of P3 could be obtained with 0.187 mg. Similarly, the number of polymer chain and Au NP were 2.57×10^{15} and 3.09×10^{14}, respectively. Finally, the grafting density of P3 could be calculated with 0.29 chains/nm^2.

8. Estimation of mass transport kinetics at the surface of working electrode

The experimental procedure involved systematic study of the potential-induced dynamic molecules transportation upon the electrode-electrolyte interface. All measurements were conducted using a customized three-electrode single cell, with a carbon rod and a saturated calomel electrode (SCE) serving as the counter and reference electrodes, respectively. The assays here were conducted using three molecular probes, including $K_3Fe(CN)_6$, Fc-COOH and $Ru(NH_3)_6Cl_3$. Afterwards, CVs were recorded for all catalysts with various scan rates from 80 to 120 mV/s. Consequently, the Randles–Ševčík equation was employed to estimate the interfacial mass transport process through diffusion coefficients of prob molecules, as seen in the following equation.[8]

$$i_p = 0.4463nFAC_O\left(\frac{nFvD_O}{RT}\right)^{\frac{1}{2}}$$

where A is the electrode surface area, F is the Faraday's constant, , R is the gas constant, T is the temperature, while n is the number of electrons involved during redox reaction. Take Au/C with $K_3Fe(CN)_6$ as an example,

$$i_p = (2.69 \times 10^5)n^{\frac{3}{2}}AD_O^{\frac{1}{2}}C_O\nu^{\frac{1}{2}}$$

$$D_O = \left(\frac{i_p}{(2.69 \times 10^5)n^{\frac{3}{2}}AC_O\nu^{\frac{1}{2}}}\right)^2$$

$$= \left(\frac{0.000329}{(2.69 \times 10^5) \times 1^{\frac{3}{2}} \times 0.1963 \times 5 \times 10^{-6}}\right)^2$$

$$= 1.6 \times 10^{-6}\ \text{cm}^2\ \text{s}^{-1}$$

Likewise, to estimate the diffusion coefficients of P1-Au/C, P2-Au/C and P3-Au/C using $K_3Fe(CN)_6$ as probe molecules, the same procedure was carried out with various scan rates under identical conditions. Therefore, the diffusion coefficients of P1-Au/C, $D_O = \left(\frac{0.000326}{(2.69\times10^5)\times1^{\frac{3}{2}}\times0.1963\times5\times10^{-6}}\right)^2 = 1.65 \times 10^{-6}$ $\text{cm}^2\ \text{s}^{-1}$; P2-Au/C $D_O = \left(\frac{0.000317}{(2.69\times10^5)\times1^{\frac{3}{2}}\times0.1963\times5\times10^{-6}}\right)^2 = 1.37 \times 10^{-6}$ $\text{cm}^2\ \text{s}^{-1}$; P3-Au/C $D_O = \left(\frac{0.000366}{(2.69\times10^5)\times1^{\frac{3}{2}}\times0.1963\times5\times10^{-6}}\right)^2 = 1.96 \times 10^{-6}$ $\text{cm}^2\ \text{s}^{-1}$. In addition, three independent measurements were carried out to get the standard deviations. For the diffusion coefficients from $Ru(NH_3)_6Cl_3$ and Fc-COOH probes, the same CVs were recorded under identical conditions except using different work

electrodes, including P2-Au/C and P3-Au/C.

For the CO_2 diffusion process, the electrochemical impedance spectroscopy (EIS) was performed in a single cell with a carbon rod and a saturated calomel electrode (SCE) served as counter and reference electrode, respectively. 0.1M $KHCO_3$ (saturated with CO_2) was used as electrolyte here during all measurements. EIS was recorded in the range of 100 kHz to 1 Hz at -0.7V vs RHE. The diffusion coefficients of CO_2 were calculated shown below.[9]

$$D = \frac{R^2T^2}{2(An^2F^2C\sigma)^2}$$

where T is the reaction temperature, at 298K, R is the gas constant (8.314 J K^{-1} mol^{-1}), n is the electrons involved in the electrocatalysis, F is the Faraday's constant, A is the surface area, ω is the angular frequency, C is the concentration of dissolved CO_2, and σ is the Warburg factor, related to the Z'.Take Au/C as an example for D_{CO2} calculation,

$$D = \frac{8.314^2 \times 298^2}{2 \times (6.93 \times 2^2 \times 96485\ .33^2 \times 1.58 \times 10^{-7} \times 1773.7)^2}$$

$$= 5.86 \times 10^{-10}\ \text{cm}^2\ \text{s}^{-1}$$

Similarly, for the nanocatalyst modified with various polymer zwitterions, including P1, P2 and P3, the EIS was carried out at -0.7V vs RHE in the range of 100 kHz to 1 Hz under identical test conditions. Warburg factors were 1659.08, 1594.11 and 1276.05 for P1-Au/C, P2-Au/C and P3-Au/C, respectively. Thus, the D_{CO2} of P1 on Au $D = \frac{8.314^2\times298^2}{2\times(6.92\times2^2\times96485\ .33^2\times1.58\times10^{-7}\times1659.1)^2} = 6.72 \times 10^{-10}$ cm^2 s^{-1}; the D_{CO2} of P2 on Au $D = \frac{8.314^2\times298^2}{2\times(5.19\times2^2\times96485\ .33^2\times1.58\times10^{-7}\times1594.1)^2} = 1.29 \times 10^{-9}$ cm^2 s^{-1}; the D_{CO2} of P3 on Au $D = \frac{8.314^2\times298^2}{2\times(4.67\times2^2\times96485\ .33^2\times1.58\times10^{-7}\times1276.0)^2} = 2.49 \times 10^{-9}$ cm^2 s^{-1}.

9. Other characterizations

The Fourier transform infrared spectroscopy (FT-IR) data was acquired using a Bruker Alpha FT-IR Spectrometer. Thermogravimetric analysis (TGA) was conducted under a nitrogen (N_2) environment using the TA Instrument TGA Q-500 facility. TGA analysis was recorded with a heat rate of 10 °C/min in the temperature range from 100 °C to 700 °C. An incubation process was performed at a temperature of 100 °C continuing 1 hour under N_2 flow to remove any residual gas contamination. The low-magnification transmission electron microscopy (TEM) was recorded using a FEI Tecnai 12 G2 Spirit BioTWIN. TEM samples were dropped casted onto a carbon-based copper grid with 400 mesh. The

TEM element mapping of nanocatalyst was performed on a JEOL 2010 TEM with an accelerating voltage at 200 kV. The transmission electron microscopy (TEM) samples were deposited onto a carbon-coated copper grid with a mesh size of 400. ^{1}H NMR spectra (500 MHz) were acquired on a Bruker Avance-500 spectrometer equipped with a prodigy probe. Gel permeation chromatography (GPC) was operated at 40 ºC using 20mM sodium trifluoroacetate in TFE as eluent at a flow rate of 1 mL/min on an Agilent 1200 series system equipped with the following: an isocratic pump, an autosampler, Polymer Standards Service (PSS) PFG guard column (8 × 50 mm), three PSS PFG analytical linear M columns (8 × 300 mm, particle size 7 μm), refractive index (RI) detection, and calibration against PMMA standards. GPC samples were filtered through a 0.45 μm PTFE filter prior to analysis. Contact angle measurements were conducted using a Biolin Scientific theta attension optical tensiometer. For the static contact angle, 2.5-μL of liquid was released onto the surface, followed by 1-min measurements at 2.3 frames per second to obtain the average results. Measurements on three different spots were collected for each sample to obtain the average value and standard deviation.

SAXS experiments were conducted by using the 16ID-LiX Beamline at the National Synchrotron Light Source II where is located at the Brookhaven National Laboratory (Upton, NY). The X-ray energy was 13.5 keV. The distance between the sample and the detector is ~ 3m, and the exposure time is 1 second. The intensity is expressed as a function of scattering vector, q defined as $\frac{4\pi}{\lambda} sin\frac{\theta}{2}$, where θ is the scattering angle and λ is the wavelength. The data covers a q range from 0.005 to 2.5 Å^{-1}. Radial averaging and q-conversion of data were analyzed by using Jupyter Notebook. SAXS model using here showed as below:

Cylindrical model:

The form factor for the cylindrical model of radius R and length L is given by:

$$F(q) = (\Delta\rho)^2(\pi R^2 L)^2 \int_0^{\pi/2} [P(q,\alpha)]^2 sin\alpha d\alpha,$$

where

$$P(q,\alpha) = \left[\frac{J_1(qRsin\alpha)}{(qRsin\alpha)} \cdot \frac{\sin(qLcos\alpha/2)}{qLcos\alpha/2}\right]$$

where α is the angle between the cylinder axis, J1 (x) is the first-order Bessel function of the first kind, and $\Delta\rho$ is the scattering length density difference between environment and materials.

Lamellar model:

The form factor of the lamellar model is expressed as below:

$$F(q) = \frac{2\Delta\rho^2}{q^2}[1 - \cos(q\delta)] = \frac{4\Delta\rho^2}{q^2} sin^2(\frac{q\delta}{2})$$

Where δ is the total layer thickness and $\Delta\rho$ is the scattering length density difference between environment and materials.

10. Molecular dynamics simulations

To understand the environment around Au-PFO-MCP solvated in aqueous CO_2 solutions of varying concentrations, MD simulations were performed using the LAMMPS software package, version 2AUG2023. The Nose-Hoover thermostat was used to maintain the temperature with a time constant of 100 fs. The polymer chains were modelled using TraPPE force field along with its extensions to phospholipid and perfluorinated alkane systems for all non-bonded, angle, and dihedral parameters except for the dihedral connecting the N-heterocyclic carbene to the monomer repeat unit which uses the AMBER86 force field. For gold atoms, non-bonded parameters were taken from the Universal Force Field (UFF), while the bond and angle parameters tethering the polymer onto the gold were taken from Nayis et al and the dihedral was taken from AMBER86. Water was modelled using the TIP4P model with the SHAKE algorithm to ensure the geometry stays rigid. CO_2 was modelled using the TraPPE forcefield and was kept rigid using an algorithm described by Kamberaj et al. Partial charges for NHC and PFO-MCP were calculated using the CM5 charge model with Gaussian16.C.01. Lorentz-Berthelot combining rules were used to resolve non-bonded interactions between unlike atoms. A spherical cutoff of 1.4 nm was used to evaluate Lennard-Jones interactions while the long-range coulombic interactions were calculated using the particle-particle-particle-mesh (PPPM) method with a relative error in forces of 10^{-4} kcal/mol/A. AuNPs represented using a 1.1 nm thick slab consisting of 864 atoms with the (111) facet exposed. The PFO-MCP chains consisted of an imidazole head, 50 isotatic PFO-MCP repeating units, and a methyl tail. Three of these chains were tethered onto the AuNP surface to reach a surface attachment of 0.29 chains/nm^2. Before solvating the system, a MD trajectory was run at 800K for 60 ns to generate six independent polymer-AuNP configurations. The remaining vacuum space above the polymer, z = 13.2 nm, to the top of the simulation box, z = 20 nm, was filled with water, generating a system of 3.4608 x 3.4608 x 20 nm^3 and 2190 water molecules. Afterwards, one or two CO_2 molecules were added into the system by replacing the same number of water molecules. For each of the CO_2 concentrations, six configurations were generated with CO_2 placed from z = 13.2 – 19.7 nm at even

spacings. These six independent configurations allow us to ensure simulation convergence regardless of the initial location CO_2 was placed in the system. To initialize the full system, energy minimization with the steepest descent algorithm was used and velocities were reinitialized to T = 700K and ran with a time step of 1 fs. The system was then allowed to equilibrate for 12 ns after which, the simulation box was cooled to 300K and the z box length was incrementally adjusted until the P_{zz} pressure averages around 1 atm, leading to a final z dimension of 17.25 nm.

Polymer	$M_{n,GPC}$/kDa	PDI_{GPC}	$M_{n,NMR}$/kDa
Poly(PFO-MCP) (P3)	13.1	1.23	43.9
Poly(HFIP-MCP) (P2)	6.7	1.25	21.5
PolyMPC (P1)	8.1	1.10	16.3

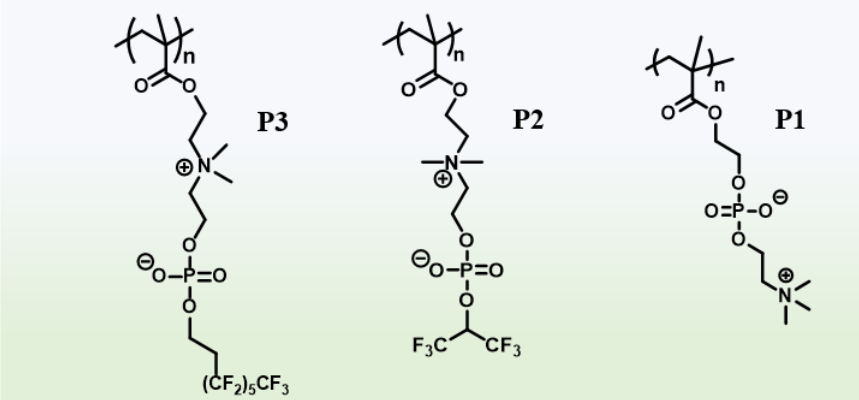

Figure S1. Summary of polyzwitterions including poly(2-methacryloyloxyethyl phosphoryl choline) (polyMPC, P1), poly(1,1,1,3,3,3-hexafluoro-2-propanol-2-methacryloyloxyethyl choline phosphate) (poly(HFIP-MCP), P2) and poly(1H,1H,2H,2H-perfluoro-1-octanol-2-methacryloyloxyethyl choline phosphate (poly(PFO-MCP), P3).

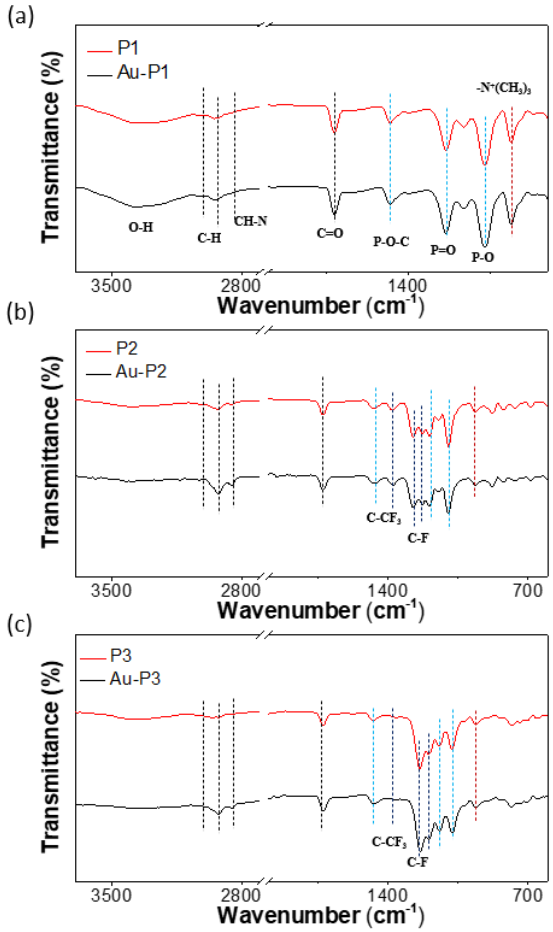

Figure S2. FT-IR spectra of pure polymer zwitterions P1 and Au NPs modified with P1, (b) P2 and Au NPs modified with P2, (c) P3 and Au NPs modified with P3.

The FT-IR spectrums of polymer zwitterions (top line) with Au NPs after polymer modifications (bottom line) were collected to confirm the surface modifications. For P1-Au NPs, as noted in blue dash line, it represented the P-O-CH_2 bending vibration at 1065 cm^{-1}, as well as the characteristic features for P=O and P-O-C at 1229 cm^{-1} and 1482 cm^{-1}. In addition, the C=O, CH-N and C-H stretching vibrations appeared at 1720 cm^{-1}, 2807 cm^{-1}, 2850 and 2930 cm^{-1} (black dash line).[10] Besides, a distinct peak appeared at 971 cm^{-1} originating from the quaternary amine head-group ($–N^+(CH_3)_3$) of P1 (dark red dash line), further indicating the modification of PMPC (P1).[10-11] Similarly, the strong stretching absorption from -CF_2- and -CF_3 in the range of 1100–1300 cm^{-1} (dark blue dash line) further implying the Au NPs were modified with P2 and P3.[12-13]

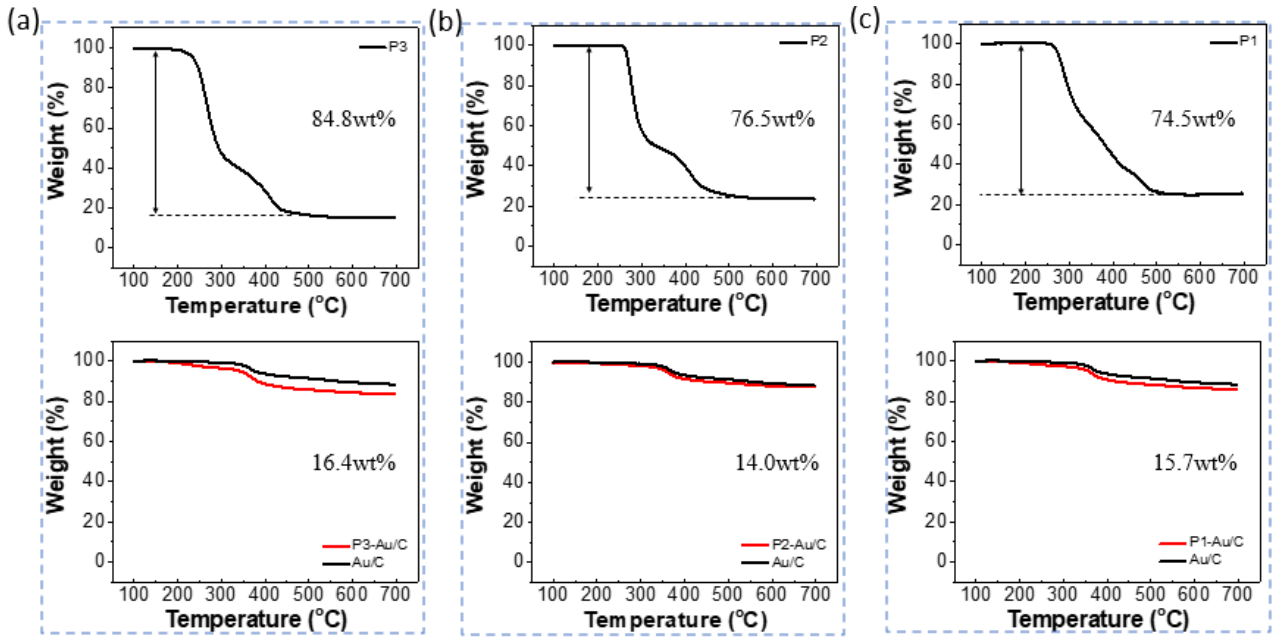

Figure S3. TGA thermograms of (a) P3 (top), P3 modified Au/C (bottom), (b) P2 (top), P2 modified Au/C (bottom) and (c) P1 (top), P1 modified Au/C (bottom).

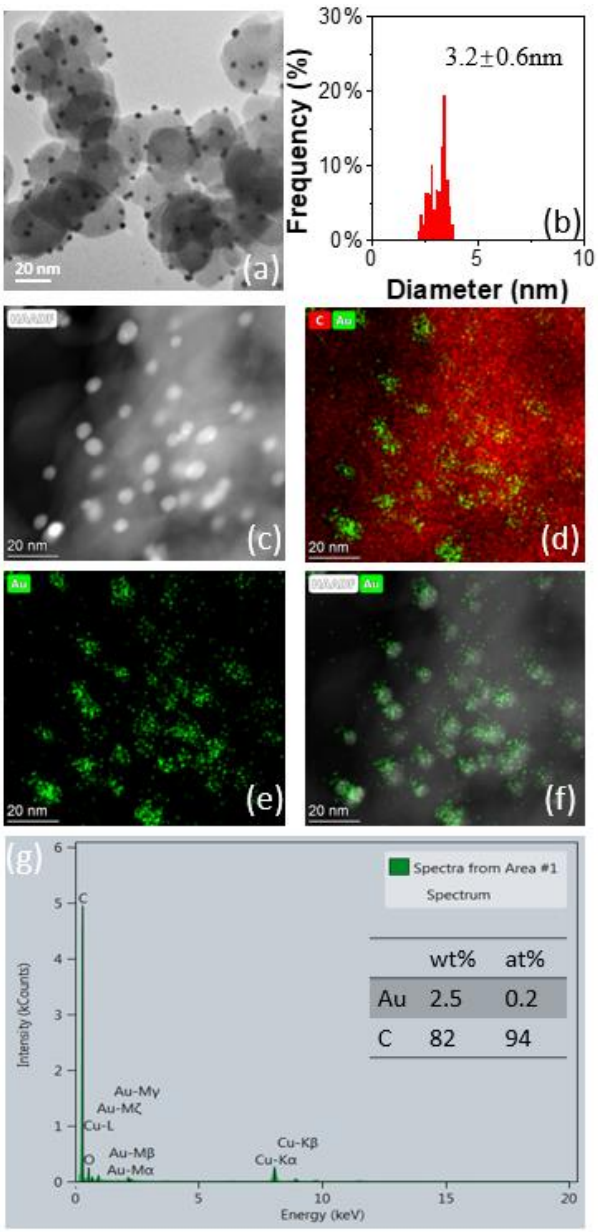

Figure S4. TEM images of Au/C (a) with corresponding size distribution histogram (b). STEM image (c) and (d-f) corresponding EDS elemental mapping image.

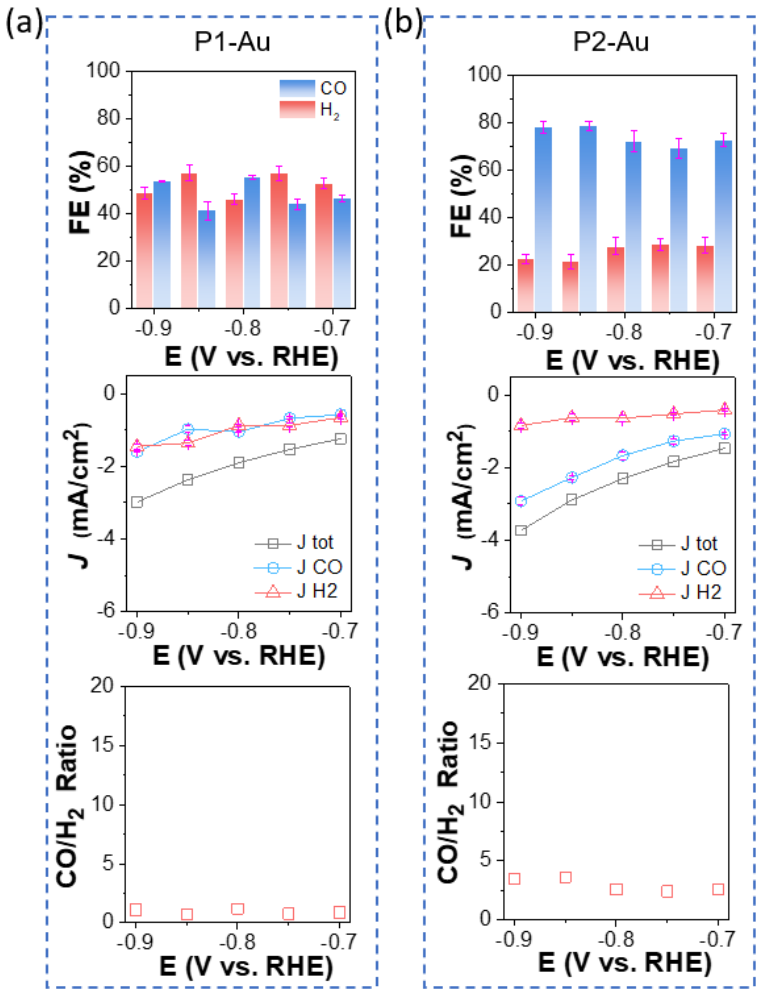

Figure S5. Electrocatalytic CO_2 reduction on ligands modified Au nanocatalysts. (a) FE (top), current density (middle) and product ratio (bottom) for P1 modified Au NPs, (b) FE (top), current density (middle) and product ratio (bottom) for P2 modified Au NPs.

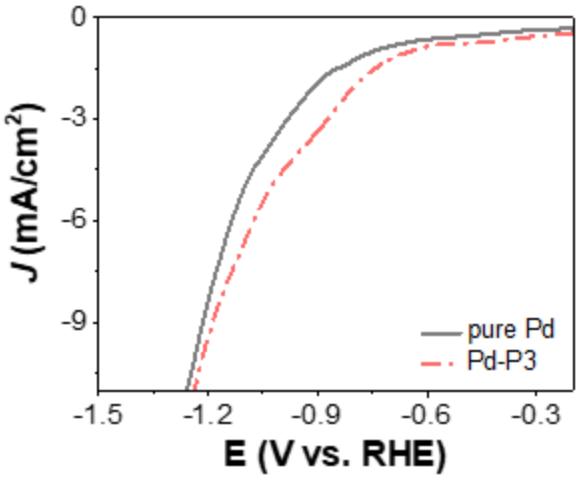

Figure S6. LSV curves measured under a scan rate of 10 mV s^{-1} in CO_2-saturated 0.1 M $KHCO_3$.

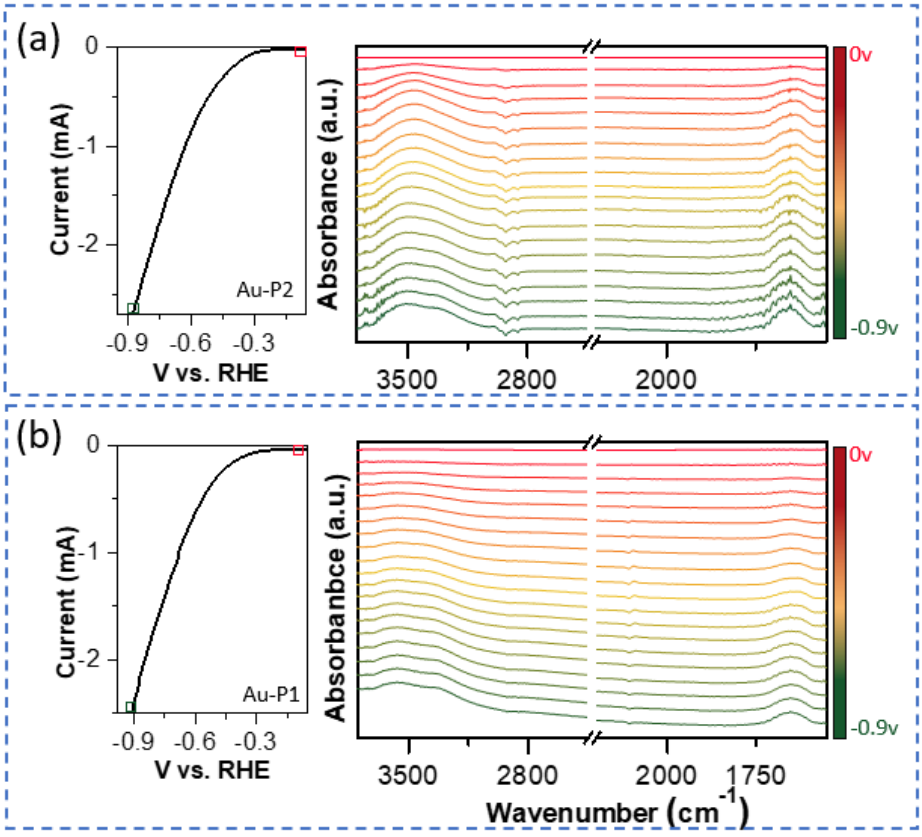

Figure S7. SEIRAS spectra of Au modified with (a) P2 and (b) P1.

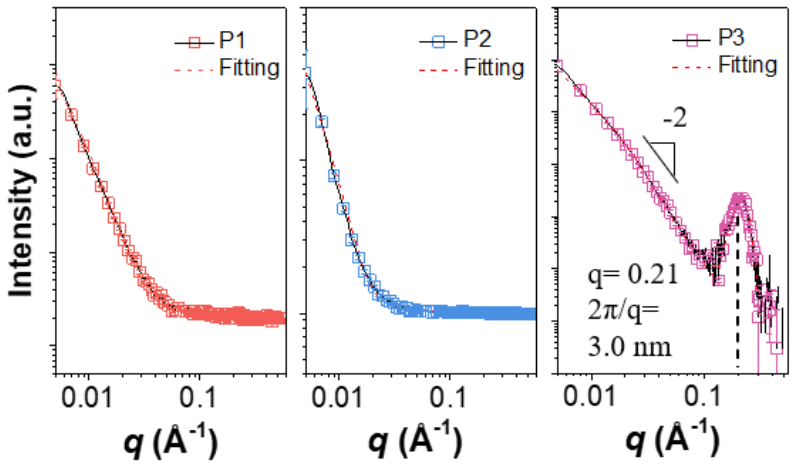

Figure S8. SAXS patterns of different fluorinated polymer zwitterions modified Au film substrate.

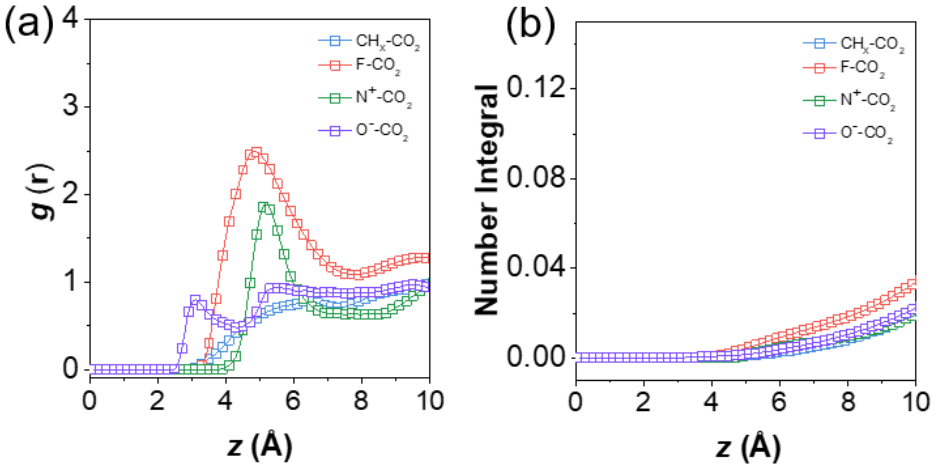

Figure S9. (a) Radial distribution function and (b) number integrals for CH_x-CO_2 between the P3 backbone and CO_2, F-CO_2 between the fluorinated tails in P3 and CO_2, N^+-CO_2 between P3 and CO_2, and O^--CO_2 between the phosphorus oxygen in P3 and CO_2.

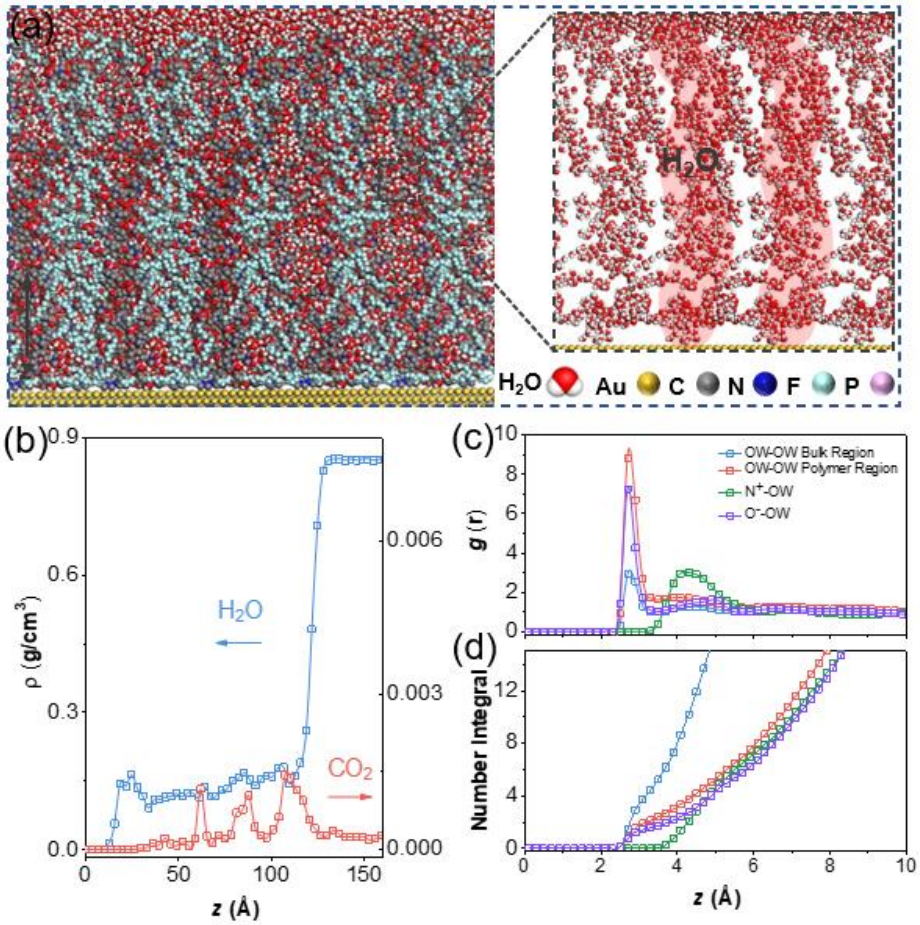

Figure S10. (a) Snapshot of a representative system configuration, with the Au, C, N, O, F, P, H atoms shown in yellow, grey, blue, red, cyan, purple, white (left) and zoomed in area of water distribution (right). (b) Density profiles as a function of z coordinates, with water and CO_2 shown in blue and red. (c) Radial distribution functions and (d) number integrals for O_W–O_W of water molecules at z > 12.76 nm (bulk region), O_W–O_W of water molecules at z < 10.95 nm (polymer layer), N^+-OW between P3 and water, O^--O_W between the phosphorous oxygen in P3 and water.

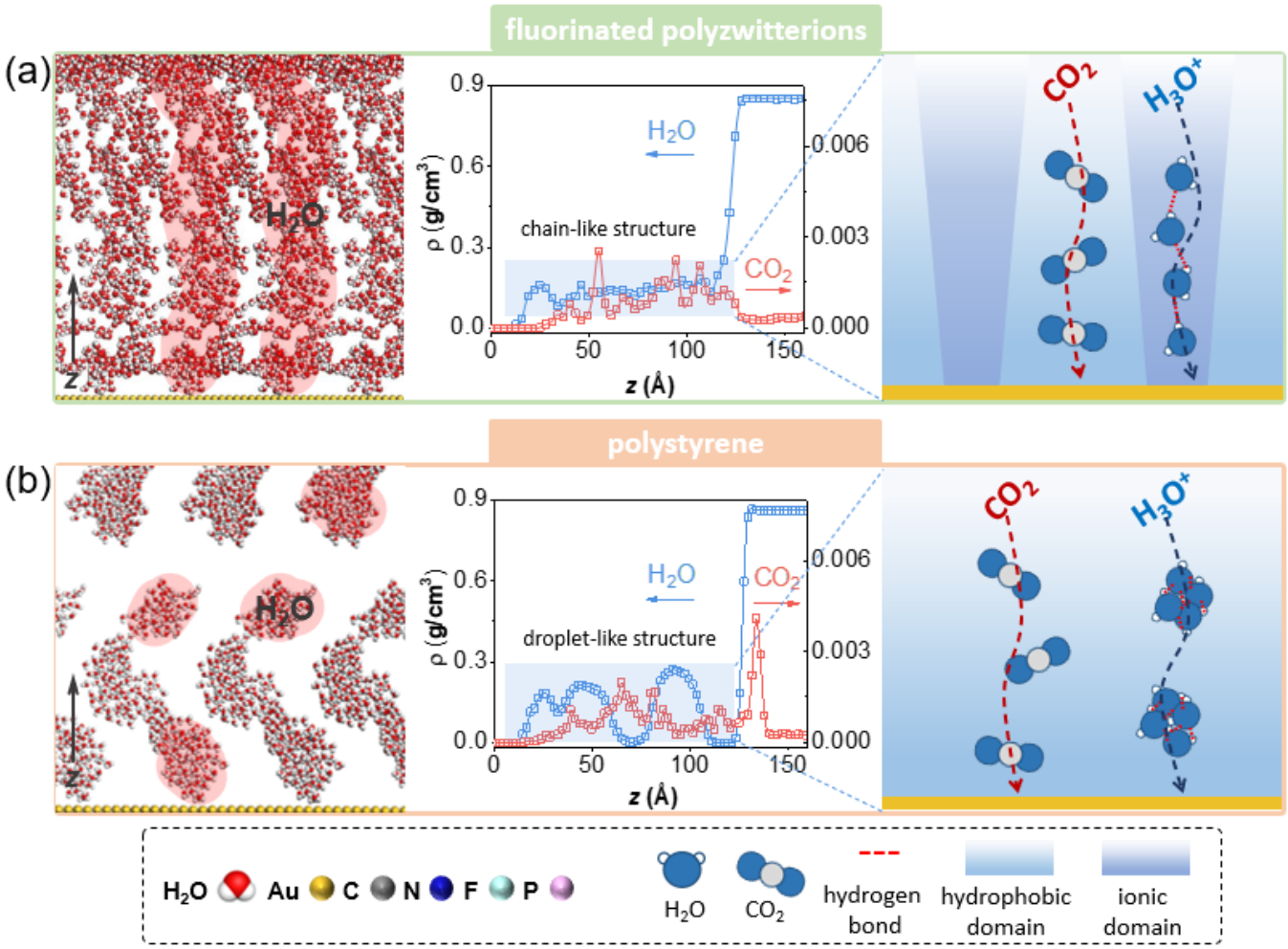

Figure S11. Comparison of water structures with various ligands. (a) Fluorinated zwitterionic ligands with a chain-like structure. (b) Hydrophobic polystyrene ligands with a more localized droplet-like structure.

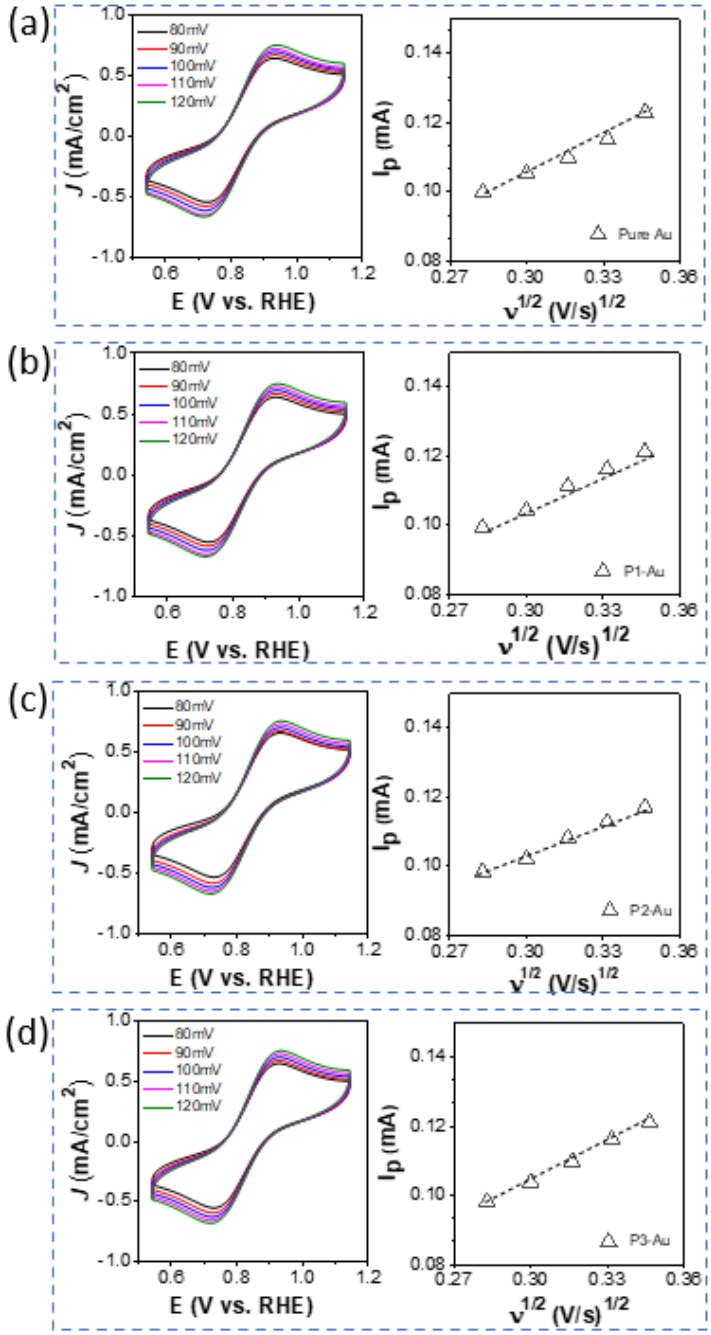

Figure S12. CV scans (left) and linear relationship between peak current (I_p) and the square root of scan rates (right) for Au NPs without ligands modification (a), P1-Au (b), P2-Au (c), and (d) P3-Au using $K_3Fe(CN)_6$ as a molecular probe.

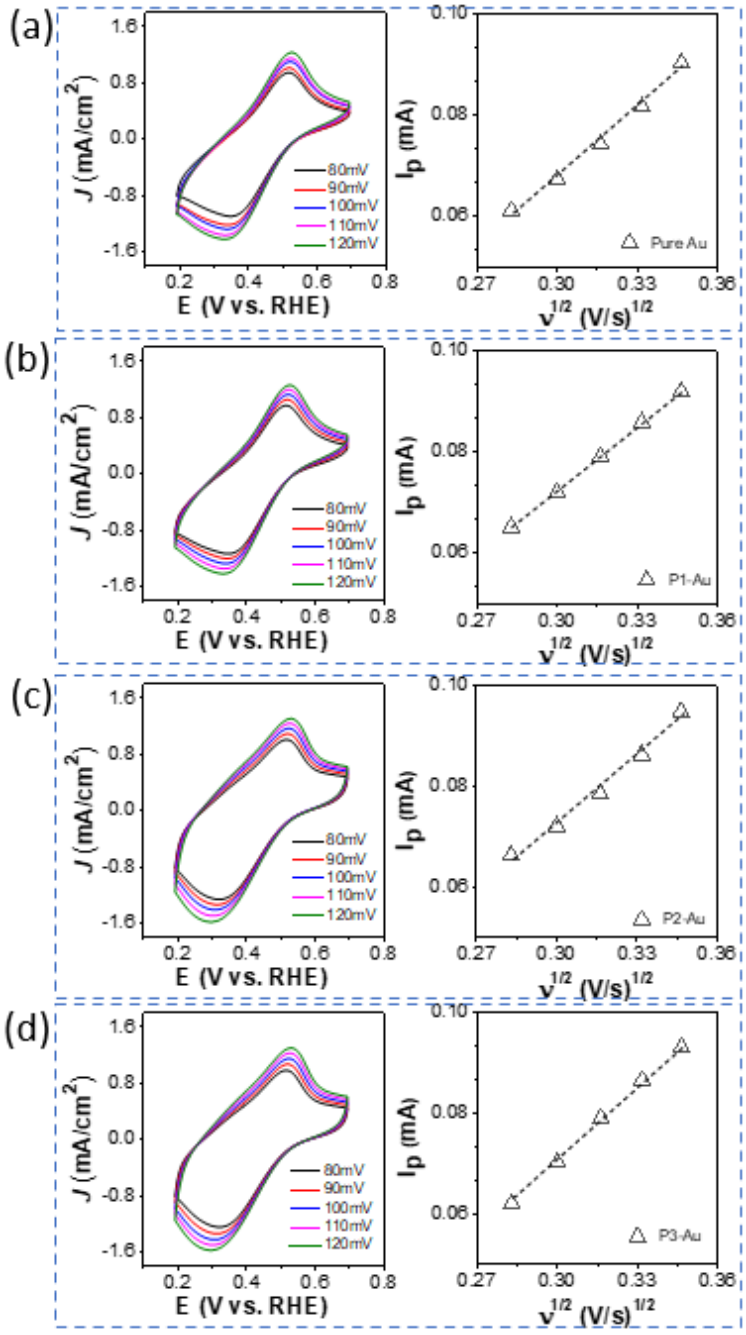

Figure S13. CV scans (left) and linear relationship between peak current (I_p) and the square root of scan rates (right) for Au NPs without ligands modification (a), P1-Au (b), P2-Au (c), and (d) P3-Au using $Ru(NH_3)_6Cl_3$ as a molecular probe.

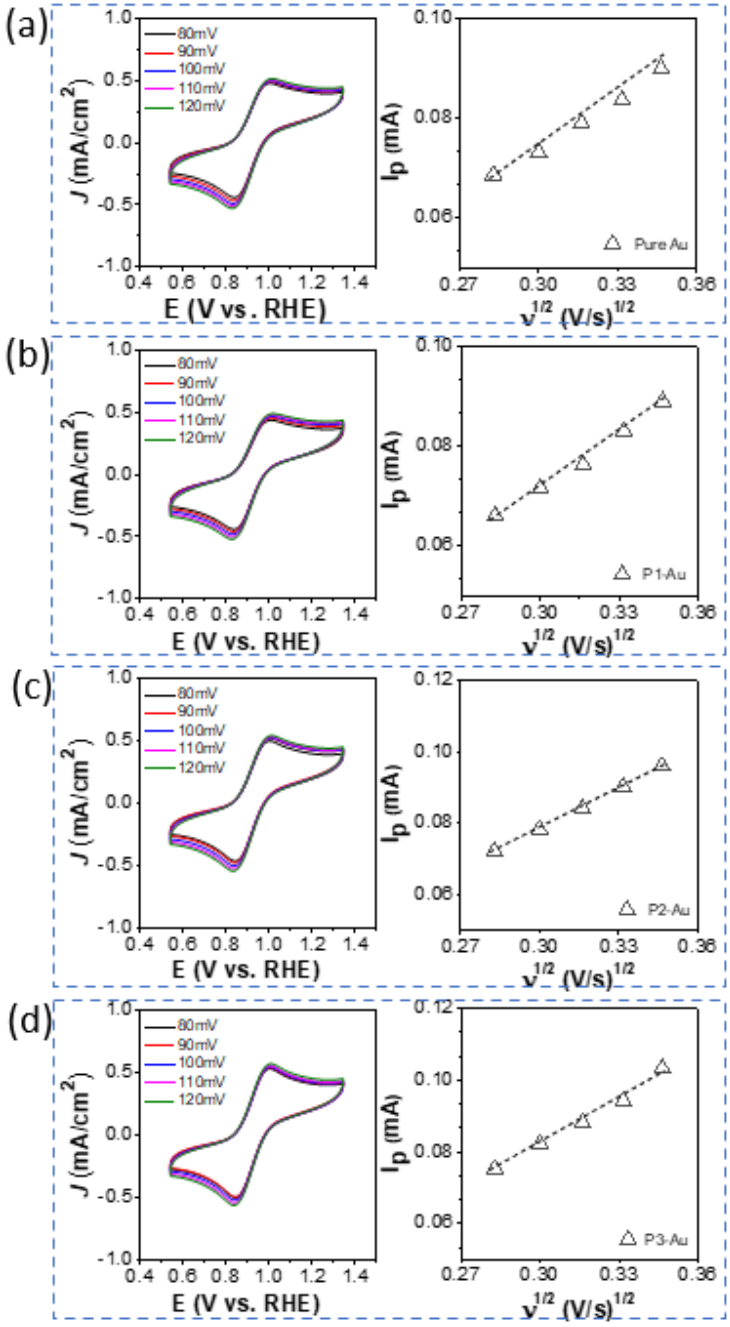

Figure S14. CV scans (left) and linear relationship between peak current (I_p) and the square root of scan rates (right) for Au NPs without ligands modification (a), P1-Au (b), P2-Au (c), and (d) P3-Au using Fc-COOH as a molecular probe.

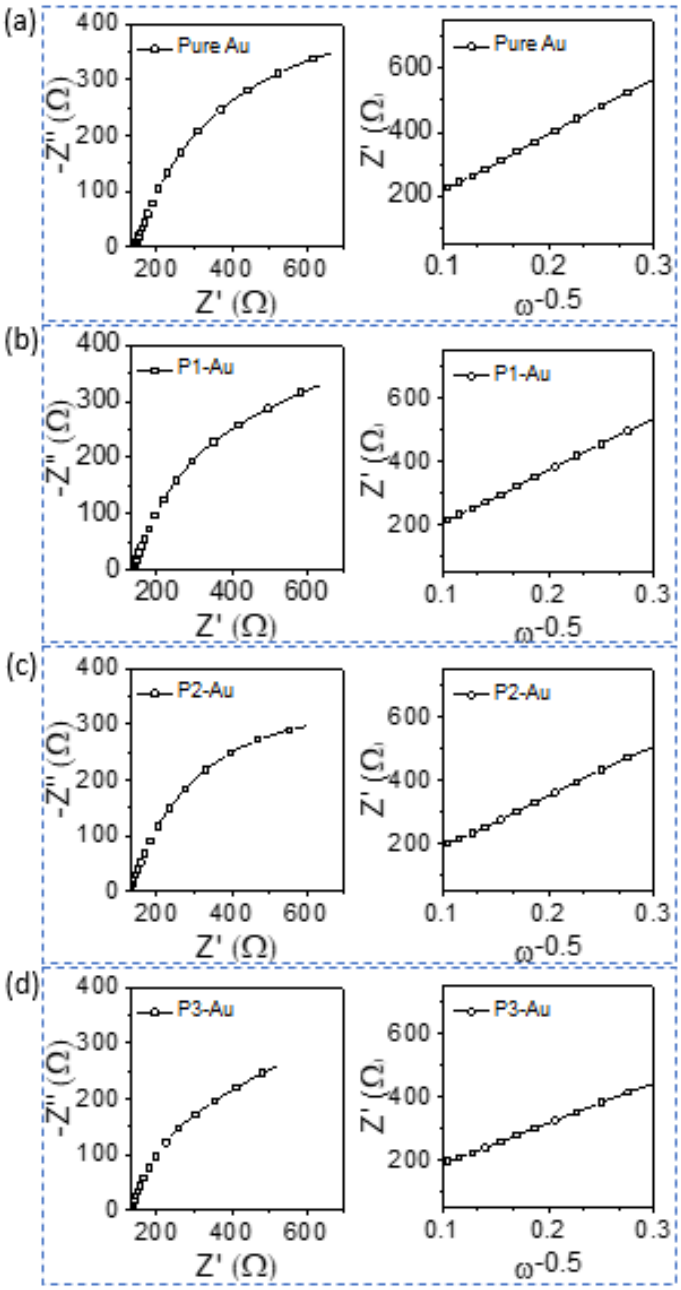

Figure S15. The EIS plots (left) and corresponding Z' against $\omega^{-0.5}$ (right) of Au/C without ligands modification and Au/C modified with various ligands including P1, P2 and P3.

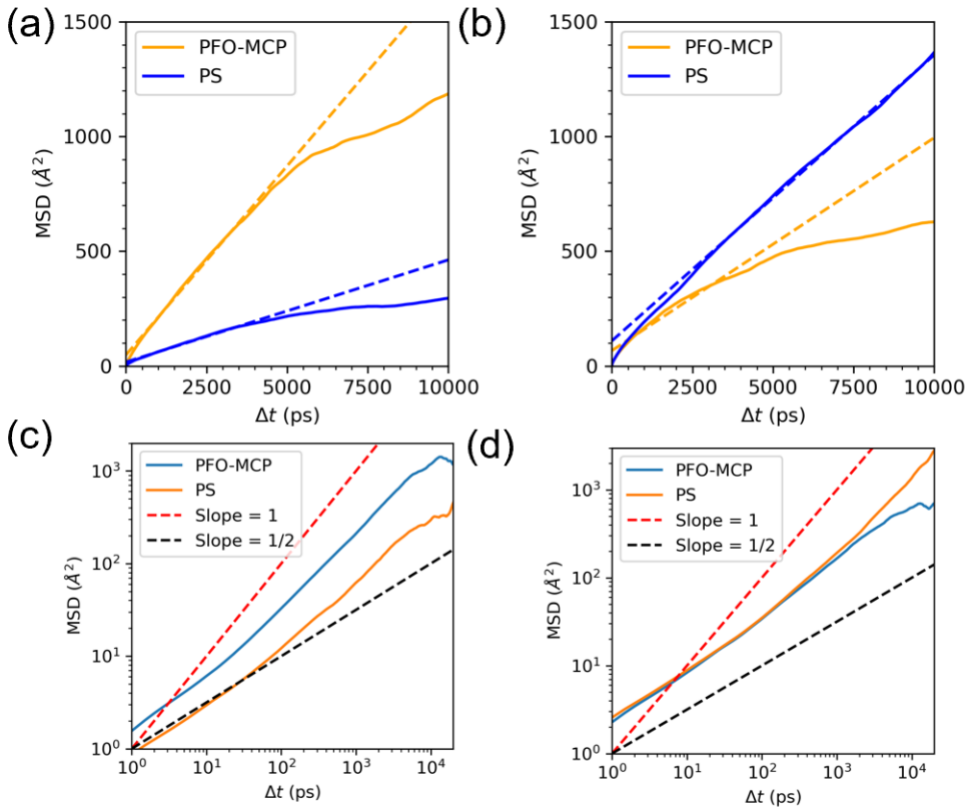

Figure S16. The linear plot of CO_2 mean-squared-displacement (Å^2) (MSD) vs time (ps) computed from the last 30 ns of the trajectory for (a) z-axis and (b) full (3-dimensional) scales. The Log-Log plot of CO_2 mean-squared-displacement (Å^2) (MSD) vs time (ps) computed from the last 30 ns of the trajectory for (c) z-axis and (d) full (3-dimensional) scales.

Table S1. Electrochemical active surface area (ECSA) estimation of Au/C without polymer modification.

Sample ID	Reduction Area C	Reference uC	Scan Rate V/s	ECSA cm^2/ug	Average cm^2/ug	STD
	7.27E-05	390	0.1	2.96		
Au	6.66E-05	390	0.1	2.71	2.75	0.19
	6.34E-05	390	0.1	2.58		

Sample ID	Reduction Area C	Reference uC	Scan Rate V/s	ECSA cm^2/ug	Average cm^2/ug	STD
	7.17E-05	390	0.1	2.92		
Au	6.69E-05	390	0.1	2.72	2.83	0.10
	6.98E-05	390	0.1	2.84		

Sample ID	Reduction Area C	Reference uC	Scan Rate V/s	ECSA cm^2/ug	Average cm^2/ug	STD
	7.46E-05	390	0.1	3.04		
Au	7.17E-05	390	0.1	2.92	2.89	0.17
	6.64E-05	390	0.1	2.70		

Sample ID	ECSA cm^2/ug	Average cm^2/ug	STD
	2.75		
Au	2.83	2.82	0.057
	2.89		

Table S2. Electrochemical active surface area (ECSA) estimation of P1-Au/C.

Sample ID	Reduction Area C	Reference uC	Scan Rate V/s	ECSA cm^2/ug	Average cm^2/ug	STD
P1-Au	6.36E-05	390	0.1	2.59	2.62	0.03
	6.50E-05	390	0.1	2.64		
	6.44E-05	390	0.1	2.62		

Sample ID	Reduction Area C	Reference uC	Scan Rate V/s	ECSA cm^2/ug	Average cm^2/ug	STD
P1-Au	6.06E-05	390	0.1	2.47	2.65	0.17
	6.89E-05	390	0.1	2.80		
	6.61E-05	390	0.1	2.69		

Sample ID	Reduction Area C	Reference uC	Scan Rate V/s	ECSA cm^2/ug	Average $cm^2/\mu g$	STD
P1-Au	6.12E-05	390	0.1	2.49	2.69	0.19
	6.71E-05	390	0.1	2.73		
	7.02E-05	390	0.1	2.86		

Sample ID	ECSA cm^2/ug	Average $cm^2/\mu g$	STD
P1-Au	2.62	2.65	0.029
	2.65		
	2.69		

Table S3. Electrochemical active surface area (ECSA) estimation of P2-Au/C.

Sample ID	Reduction Area C	Reference uC	Scan Rate V/s	ECSA cm^2/ug	Average $cm^2/\mu g$	STD
P2-Au	4.80E-05	390	0.1	1.95	2.06	0.09
	5.24E-05	390	0.1	2.13		
	5.15E-05	390	0.1	2.10		

Sample ID	Reduction Area C	Reference uC	Scan Rate V/s	ECSA cm^2/ug	Average $cm^2/\mu g$	STD
P2-Au	4.61E-05	390	0.1	1.88	2.05	0.15
	5.12E-05	390	0.1	2.08		
	5.35E-05	390	0.1	2.18		

Sample ID	Reduction Area C	Reference uC	Scan Rate V/s	ECSA cm^2/ug	Average $cm^2/\mu g$	STD
P2-Au	4.64E-05	390	0.1	1.89	2.03	0.12
	5.09E-05	390	0.1	2.07		
	5.21E-05	390	0.1	2.12		

Sample ID	ECSA cm^2/ug	Average $cm^2/\mu g$	STD
P2-Au	2.06	2.05	0.013
	2.05		
	2.03		

Table S4. Electrochemical active surface area (ECSA) estimation of P3-Au/C.

Sample ID	Reduction Area C	Reference uC	Scan Rate V/s	ECSA cm^2/ug	Average cm^2/ug	STD
P3-Au	4.73E-05	390	0.1	1.93	1.85	0.07
	4.53E-05	390	0.1	1.84		
	4.41E-05	390	0.1	1.79		

Sample ID	Reduction Area C	Reference uC	Scan Rate V/s	ECSA cm^2/ug	Average cm^2/ug	STD
P3-Au	4.61E-05	390	0.1	1.88	1.87	0.05
	4.46E-05	390	0.1	1.82		
	4.71E-05	390	0.1	1.92		

Sample ID	Reduction Area C	Reference uC	Scan Rate V/s	ECSA cm^2/ug	Average cm^2/ug	STD
P3-Au	4.72E-05	390	0.1	1.92	1.88	0.04
	4.51E-05	390	0.1	1.84		
	4.61E-05	390	0.1	1.88		

Sample ID	ECSA cm^2/ug	Average $cm^2/\mu g$	STD
P3-Au	1.85	1.87	0.012
	1.87		
	1.88		

Table S5. Electrochemical CO_2 reduction with Au NPs modified with polymer zwitterions and other reported Au catalysts.

Catalysts	Electrolyte	FE_{CO} (V vs RHE)	References
P3-Au NPs (3.2 nm)	0.1 M $KHCO_3$	91.3±7.2% (-0.8 V)	This work
Au NPs (4 nm)	0.5 M $NaHCO_3$	61% (-0.78 V)	14
Au NPs (6 nm)	0.5 M $NaHCO_3$	71% (-0.78 V)	14
Au NPs (10 nm)	0.5 M $NaHCO_3$	68% (-0.78 V)	14
Au NWs (100 nm)	0.5 M $NaHCO_3$	78% (-0.8 V)	15
Au NWs (15 nm)	0.5 M $NaHCO_3$	65% (-0.8 V)	15
$[Au_{22}H_3(PPh_3)_8(dppe)_3]Cl_3$	0.5 M $KHCO_3$	71% (-0.8 V)	16
$[Au_{11}(dppe)_5]Cl_3$	0.5 M $KHCO_3$	63% (-0.8 V)	16
$Au_{2\ nm}$	0.1 M $NaHCO_3$	8±1% (-0.50 V)	17
$Au_{5\ nm}$	0.1 M $NaHCO_3$	11±2% (-0.56 V)	17
$Au_{25\ nm}$ nanorod	0.5 M $KHCO_3$	28% (-0.57V)	18
$Au_{25\ nm}$ nanosphere	0.5 M $KHCO_3$	73.7% (-0.57 V)	18

Table S6. Faradic efficiency data of Pd and P3-Pd catalysts.

Sample ID	Potential (V vs RHE)	FE of CO			Average	STD
Pd	-0.7	34.2	30.1	28.4	30.9	2.4
	-0.75	30.7	38.5	42.5	37.2	4.9
	-0.8	42.4	48.7	41.7	44.3	3.1
	-0.85	34.4	33.1	39.7	35.7	2.9
	-0.9	42.6	36.7	44.2	41.2	3.2

Sample ID	Potential (V vs RHE)	FE of H_2			Average	STD
Pd	-0.7	67.3	71.3	73.1	70.6	2.4
	-0.75	70.6	69.7	59.4	66.6	5.1
	-0.8	56.4	50.2	58.1	54.9	3.4
	-0.85	67.2	68.3	62.6	66.0	2.5
	-0.9	59.3	64.7	57.3	60.4	3.1

Sample ID	Potential (V vs RHE)	FE of CO			Average	STD
P3-Pd	-0.7	42.8	43.4	38.7	41.6	2.1
	-0.75	47.3	41.1	48.8	45.7	3.3
	-0.8	54.9	52.7	51.7	53.1	1.3
	-0.85	46.2	47.5	41.2	44.9	2.7
	-0.9	48.3	49.8	50.6	49.6	1.0

Sample ID	Potential (V vs RHE)	FE of H_2			Average	STD
P3-Pd	-0.7	56.9	55.7	61.9	58.2	2.7
	-0.75	58.7	56.3	56.8	57.3	1.0
	-0.8	47.2	44.2	48.6	46.7	1.8
	-0.85	56.1	58.3	60.2	58.2	1.7
	-0.9	53.2	50.4	51.8	51.8	1.1

Reference in SI

1. Zhou, L.; Triozzi, A.; Figueiredo, M.; Emrick, T., Fluorinated Polymer Zwitterions: Choline Phosphates and Phosphorylcholines. *ACS Macro Lett* **2021,** *10* (10), 1204-1209.
2. Zhou, L.; Yang, Z.; Pagaduan, J. N.; Emrick, T., Fluorinated zwitterionic polymers as dynamic surface coatings. *Polymer Chemistry* **2023,** *14* (1), 32-36.
3. Jana, N. R.; Gearheart, L.; Murphy, C. J., Seeding Growth for Size Control of 5−40 nm Diameter Gold Nanoparticles. *Langmuir* **2001,** *17* (22), 6782-6786.
4. Dunwell, M.; Yan, Y.; Xu, B., A surface-enhanced infrared absorption spectroscopic study of pH dependent water adsorption on Au. *Surface Science* **2016,** *650*, 51-56.
5. Dunwell, M.; Lu, Q.; Heyes, J. M.; Rosen, J.; Chen, J. G.; Yan, Y.; Jiao, F.; Xu, B., The Central Role of Bicarbonate in the Electrochemical Reduction of Carbon Dioxide on Gold. *Journal of the American Chemical Society* **2017,** *139* (10), 3774-3783.
6. Sukeri, A.; Saravia, L. P. H.; Bertotti, M., A facile electrochemical approach to fabricate a nanoporous gold film electrode and its electrocatalytic activity towards dissolved oxygen reduction. *Physical Chemistry Chemical Physics* **2015,** *17* (43), 28510-28514.
7. Zhang, L.; Wei, Z.; Thanneeru, S.; Meng, M.; Kruzyk, M.; Ung, G.; Liu, B.; He, J., A Polymer Solution To Prevent Nanoclustering and Improve the Selectivity of Metal Nanoparticles for Electrocatalytic CO2 Reduction. *Angewandte Chemie International Edition* **2019,** *58* (44), 15834-15840.
8. Rodríguez Presa, M. J.; Gassa, L. M.; Azzaroni, O.; Gervasi, C. A., Estimating Diffusion Coefficients of Probe Molecules into Polyelectrolyte Brushes by Electrochemical Impedance Spectroscopy. *Analytical Chemistry* **2009,** *81* (19), 7936-7943.
9. Li, S.; Xu, Q.; Uchaker, E.; Cao, X.; Cao, G., Comparison of amorphous, pseudohexagonal and orthorhombic Nb2O5 for high-rate lithium ion insertion. *CrystEngComm* **2016,** *18* (14), 2532-2540.
10. Zhu, L.; Jin, Q.; Xu, J.; Ji, J.; Shen, J., Poly(2-(methacryloyloxy) ethyl phosphorylcholine)-functionalized multi-walled carbon nanotubes: Preparation, characterization, solubility, and effects on blood coagulation. *Journal of Applied Polymer Science* **2009,** *113* (1), 351-357.
11. Jiang, L.; Zhu, W.; Qian, H.; Wang, C.; Chen, Y.; Liu, P., Fabrication of PMPC/PTM/PEGDA micropatterns onto polypropylene films behaving with dual functions of antifouling and antimicrobial activities. *Journal of Materials Chemistry B* **2019,** *7* (33), 5078-5088.
12. Rodrigues, I. C. P.; Woigt, L. F.; Pereira, K. D.; Luchessi, A. D.; Lopes, É. S. N.; Webster, T. J.; Gabriel, L. P., Low-cost hybrid scaffolds based on polyurethane and gelatin. *Journal of Materials Research and Technology* **2020,** *9* (4), 7777-7785.
13. Zhao, M.; Yu, Y.; Han, Z.; Li, H. Preparation of a Fluorocarbon Polymerizable Surfactant and Its Application in Emulsion Polymerization of Fluorine-Containing Acrylate *Polymers* [Online], 2017.
14. Zhu, W.; Michalsky, R.; Metin, Ö.; Lv, H.; Guo, S.; Wright, C. J.; Sun, X.; Peterson, A. A.; Sun, S., Monodisperse Au Nanoparticles for Selective Electrocatalytic Reduction of CO2 to CO. *Journal of the American Chemical Society* **2013,** *135* (45), 16833-16836.
15. Zhu, W.; Zhang, Y.-J.; Zhang, H.; Lv, H.; Li, Q.; Michalsky, R.; Peterson, A. A.; Sun, S., Active and Selective Conversion of CO2 to CO on Ultrathin Au Nanowires. *Journal of the American Chemical Society* **2014,** *136* (46), 16132-16135.
16. Gao, Z.-H.; Wei, K.; Wu, T.; Dong, J.; Jiang, D.-e.; Sun, S.; Wang, L.-S., A Heteroleptic Gold Hydride Nanocluster for Efficient and Selective Electrocatalytic Reduction of CO2 to CO. *Journal of the American Chemical Society* **2022,** *144* (12), 5258-5262.
17. Kauffman, D. R.; Alfonso, D.; Matranga, C.; Qian, H.; Jin, R., Experimental and Computational Investigation of Au25 Clusters and CO2: A Unique Interaction and Enhanced Electrocatalytic Activity. *Journal of the American Chemical Society* **2012,** *134* (24), 10237-10243.
18. Cai, X.; Li, G.; Hu, W.; Zhu, Y., Catalytic Conversion of CO2 over Atomically Precise Gold-Based Cluster Catalysts. *ACS Catalysis* **2022,** *12* (17), 10638-10653.